University of Bath

1

The Synthesis and Materials Chemistry of Bismuth *Tris*-(di-i-propylcarbamate) : Deposition of Photoactive Bi$_2$O$_3$ Thin Films

Samuel D Cosham, Michael S Hill, Graeme A Horley, Andrew L Johnson, Laura Jordan, Kieran C Molloy* and David C Stanton

Department of Chemistry, University of Bath, Claverton Down, Bath, BA2 7AY, UK

Abstract

The bismuth carbamate Bi(O$_2$CNPr$^i_2$)$_3$, a tetramer in the solid-state, has been synthesised and used to deposit mixtures of bismuth oxides by aerosol-assisted chemical vapour deposition (AACVD). The nature of the deposited oxide is a function of both temperature and run-time. Initially, δ-Bi$_2$O$_3$ is deposited, over which grows a thick layer of β-Bi$_2$O$_3$ nanowires, the latter having an increasing degree of preferred orientation at higher deposition temperatures. The photocatalytic activity of a thin film of δ-Bi$_2$O$_3$ for the degradation of methylene blue dye was found to be similar to that of a commercial TiO$_2$ film on glass, while the film overcoated with β-Bi$_2$O$_3$ nanowires was less active. Exposure of Bi(O$_2$CNPr$^i_2$)$_3$ to controlled amounts of moist air affords the novel oxo-cluster Bi$_8$(O)$_6$(O$_2$CNPr$^i_2$)$_{12}$, whose structure has also been determined.

Keywords: Bismuth, carbamate, oxide, oxo-cluster, thin film, photocatalyst

Introduction

Carbamates ($R_2NCO_2^-$) are an interesting class of ligand which form a link between carboxylates (RCO_2^-) and dithiocarbamates ($R_2NCS_2^-$). They have been widely studied as metal complexes across most of the Periodic Table,[1] though surprisingly only one brief report has appeared concerning bismuth.[2] Beyond the structural interest, carbamates (or isomers thereof) offer an alternative ligand for the formation of potentially volatile precursors for chemical vapour deposition (CVD),[3, 4] and in this regard the two substituents on nitrogen offer additional opportunities for steric crowding, in comparison with, for example, carboxylates. Bismuth carbamates are, therefore, possible precursors for Bi_2O_3, a material exploited either alone[5] or, more significantly, as a component of more complex materials such as $Bi_2Sn_2O_7$ (catalyst, CO sensor),[6, 7] $BiFeO_3$ (a multiferroic compound),[8] $Bi_4YTi_3O_{12}$ and $SrBi_2Ta_3O_9$ (ferroelectric perovskites) [9, 10] and $Bi_2Sr_2CaCu_2O_8$ (high temperature superconductor).[11] Existing CVD precursors for bismuth oxides include BI_3,[12-18] $Bi(NO_3)_{3,}$[19] $BiPh_3$[20-22] and related bismuth aryls[23] and alkyls,[24] β-diketonates such as $Bi(thd)_3$ (thd = tetramethylheptane-dione),[23, 25, 26] and both simple and functionalised alkoxides,[27-29] all summarised in refs. 5 and 28. However, of these only the three alkoxides[27-29] are single-source precursors (SSPs), the remainder requiring a co-reactant, usually O_2.

In this paper we report the first structural characterisation of a bismuth carbamate, and its controlled hydrolysis to an unusual Bi_8-oxo cluster, along with use of the carbamate as a CVD precursor for photoactive Bi_2O_3 thin films.

Experimental Section

General Procedures: All operations were performed under an atmosphere of dry argon using standard Schlenk line and glovebox techniques. Hexanes were dried using a commercially available solvent purification system (Innovative Technology Inc., MA, USA) and degassed under argon prior to use. Tetrahydrofuran (THF) was dried by refluxing over potassium before isolating by distillation and degassing under argon prior to use. Deuterated benzene (C_6D_6) and deuterated chloroform ($CDCl_3$) NMR solvents were purchased from Fluorochem, UK, and dried by refluxing over potassium and over 4 Å molecular sieves respectively, before isolating *via* vacuum distillation. All dry solvents were stored under

argon in Young's ampoules over 4 Å molecular sieves. $BiCl_3$ and 2M solution of $LiNPr^i_2$ were purchased

from commercial sources and used as received. $Bi(NPr^i_2)_3$ was prepared by a literature procedure.[30]

Melting points were determined utilising a Stuart SMP10 Melting Point Apparatus. Elemental analyses

were performed externally by London Metropolitan University Elemental Analysis Service, UK. Solution ^1H

and $^{13}C\{^1H\}$ NMR spectra were recorded with a Bruker Avance 300 spectrometer at ambient temperature

(25 ^oC). ^1H and ^{13}C NMR chemical shifts are referenced internally to residual non-deuterated solvent

resonances. All chemical shifts are reported in δ (ppm) and coupling constants in Hz. The following

abbreviations are used: d (doublet), m (multiplet) and br (broad).

Synthesis of $Bi(O_2CNPr^i_2)_3$ (1). Dry CO_2 was slowly bubbled through a stirred solution of $Bi(NPr^i_2)_3$

(0.510 g, 1 mmol) in hexanes (15 mL) for 30 minutes. Crystallisation from the reaction solution at -28 °C

yielded the desired product as small colourless crystals. Yield = 0.526 g, 83%.

Alternatively, the same compound can be prepared in a one-pot synthesis, as follows. A stirred

suspension of $BiCl_3$ (8.514 g, 27 mmol) in THF (100 mL) was slowly treated at -78 ^oC with a 2M THF/*n*-

heptane/ethylbenzene solution of $LiNPr^i_2$ (42.0 mL, 84 mmol). The reaction solution was slowly allowed to

warm to ambient temperature and stirred for 4 h, before volatiles were removed *in vacuo*. To the residue,

hexanes (150 mL) were added and the resultant solution filtered through Celite. Dry CO_2 was then slowly

bubbled through the solution for 1 h, with subsequent crystallisation from the reaction solution at -28 ^oC

yielding the desired product as colourless crystals. Yield: 11.96 g, 69%. m.p. 91 - 92 ^oC. Analysis, found

(calculated for $C_{21}H_{42}BiN_3O_6$): C 39.46 (39.31), H 6.52 (6.60), N 6.68 (6.55)%. ^1H NMR (300 MHz, C_6D_6):

$δ_H$ 3.92 (br m, 1H, C*H*CH$_3$), 1.28 (d, 6H, CHC*H*$_3$, $^3J_{CHCH3}$ 6.6). $^{13}C\{^1H\}$ NMR (75.5 MHz, C_6D_6): $δ_C$ 163.6

(N*C*O$_2$), 45.9 (*C*H), 21.2 (*C*H$_3$).

Synthesis of $Bi_8(O)_6(O_2CNPr^i_2)_{12}$ (2). A hexanes solution containing **1** was prepared as described above

before volatiles were subsequently removed *in vacuo*. The resultant residue was dissolved in THF (15

mL) and the solution was then filtered. Compound **2** was obtained as colourless crystals by crystallisation

from this reaction solution upon partial exposure to the ambient atmosphere for 72 h. Yield: 0.09 g, 21%.

m.p. 204 - 208 ^oC (dec.). Analysis, found (calculated for $C_{84}H_{168}Bi_8N_{12}O_{30}$): C 28.81 (28.84), H 4.75 (4.84),

N 4.77 (4.80)%. ^{1}H NMR (300 MHz, CDCl$_3$): δ$_H$ 4.33-3.60 (br m, 3H, CHCH$_3$), 2.98-2.83 (m, 1H, CHCH$_3$), 1.23 (d, 6H, CHCH_3, ^{3}J$_{CHCH3}$ 6.3), 1.19-1.07 (m, 12H, CHCH_3), 1.04 (d, 6H, CHCH_3, ^{3}J$_{CHCH3}$ 6.2). ^{13}C{^{1}H} NMR (75.5 MHz, CDCl$_3$): δ$_C$ 162.9, 161.8 (NCO$_2$), 45.3 (CH), 21.2, 21.1, 21.0 (CH$_3$).

DOSY NMR Procedure:

Diffusion experiments were performed for 1 M and saturated solutions of **1** in dried d$_8$-toluene and were recorded at 298 K and 353 K on a Bruker Avance 400 spectrometer operating at 400.13 MHz for ^{1}H. Experiments were performed using a double stimulated echo pulse sequence to allow for convection compensation, with Δ of 50 ms and δ of 2 ms. Gradient strengths were incremented linearly, in eight steps, from 1.74 to 33.14 Gcm^{-1}, with 16 scans recorded at each gradient strength. Diffusion coefficients were calculated using Bruker's inbuilt T1/T2 software. The hydrodynamic radius (r) of **1** was calculated using the Stokes-Einstein equation:

$$r = \frac{k_B T}{6\pi\eta D}$$

where k_B is the Boltzmann constant, T is the temperature, η is the viscosity of the solution and D is the diffusion coefficient.

Crystallography

Experimental details relating to the single-crystal X-ray crystallographic studies are summarised in Table 1. For all structures, data were collected on a Nonius Kappa CCD diffractometer at 150(2) K using Mo-K$_\alpha$ radiation (λ = 0.71073 Å). Structure solution followed by full-matrix least squares refinement was performed using the WinGX-1.70 suite of programmes.[31] Corrections for absorption (multi-scan) were made in both cases. The asymmetric unit of **1** consists of one quarter of the tetrameric complex and a co-crystallised solvent molecule at half occupancy. This latter has been modelled as pentane, though symmetry places two such molecules in close proximity. It is likely that the solvent present is a mixture of hexane isomers (*see* the synthetic protocol), though we have made no further effort to model this aspect of the structure given its relative unimportance. Bond lengths and angles in the solvent molecule have

been geometrically fixed and C(35) is refined isotropically. **2**: The asymmetric unit contains three THF molecules (6 per Bi_8 cluster), one of which is disordered over two sites in a 87:13 ratio.

Materials Chemistry

Thermogravimetric analyses (TGA) were performed either at SAFC HiTech, Bromborough, UK, using a Shimadzu TGA-51 Thermogravimetric Analyzer (**1**), or at Bath using a TA Instruments Q500 TGA instrument (**2**). Data points were collected every second at a ramp rate of 10 ^{o}C min^{-1} in a flowing (90 mL min^{-1}) N_2 stream.

Film depositions were carried out at atmospheric pressure in a cold-wall Electrogas reactor containing a graphite heating block on which the substrate is situated. The precursor was injected as a 0.05 M hexanes solution (20 mL) into a glass flask sitting in an ultrasonic nebulizer, located just before the reactor chamber. Prior to injecting the precursor, the chamber was loaded with the substrate and heated under a flow of preheated nitrogen (0.8 L/min, 120 ^{o}C) to the required temperature before allowing it to equilibrate for at least 30 min. The precursor was then injected and the nebulizer started to begin the deposition. Films were deposited on glass substrates at 300 ^{o}C for run times of 10 min (R1) and 40 min (R2), at 375 ^{o}C for 40 min (R3) and at 450 ^{o}C for 40 min (R4). After each deposition, the films were allowed to cool slowly to ambient temperature under a flow of nitrogen. The glass substrates (glass microscope slides) were cleaned *via* sonication in Piranha solution, rinsed with deionized water and dried under a flow of N_2 prior to loading into the chamber.

Photocatalysis studies

The photocatalytic activities of the δ- and β-Bi_2O_3 films were evaluated by the decolorization of methylene blue (MB). A 200 W HMI HR lamp (AM 1.5, 1 Sun, 735 Wm^{-2}) was used as a light source to provide broad wavelength solar irradiation. The experiments were performed under ambient temperature as follows: In each run, the photoactive film (2.5 cm^2) was placed in a glass vessel and submerged in 10ml of MB solution (1x10^{-5} mol L^{-1}). Before illumination, the solution was stirred for 30 min in the dark to equilibriate adsorption-desorption of MB and photocatalyst. The solution was then stirred and exposed to

solar irradiation. The concentration of the MB was monitored by measurement of the absorbance at 665

nm during the photodegradation process using a Varian Cary 50 UV-Visible spectrophotometer.

Table 1. Crystal data and structure refinement for **1** and **2**

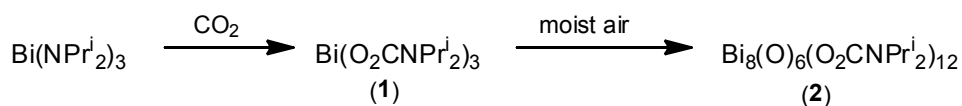| Identification code	**1**	**2**
Empirical formula	$C_{94}H_{192}Bi_4N_{12}O_{24}$	$C_{108}H_{216}Bi_8N_{12}O_{36}$
Formula weight	2710.52	3930.77
Crystal system	Tetragonal	Monoclinic
Space group	$P42_1c$	$P2_1/n$
a (Å)	19.5893(1)	16.1210(2)
b (Å)	19.5893(1)	27.1155(3)
c (Å)	15.6809(1)	16.8963(3)
β (^{0})		105.4263(7)
V (Å^3)	6017.40(6)	7119.77(17)
Z	2	2
ρ_{calc} (Mgm^{-3})	1.496	1.834
μ(Mo-k$_\alpha$) (mm^{-1})	5.897	9.921
F(000)	2728	3800
Crystal size (mm)	0.25 x 0.25 x 0.20	0.20 x 0.12 x 0.08
Theta range	4.83 to 30.03 deg.	3.84 to 30.20 deg.
Reflections collected	121369	93257
Independent refl'{R(int)]	8761 [0.0611]	19721 [0.1093]
Refl'ns observed (>2σ)	8163	13013
Data Completeness (%)	99.3	93.2
Max., min. transmission	0.3851, 0.3203	0.5041, 0.2416
Goodness-of-fit on F^2	1.086	1.012
Final R$_1$, wR$_2$ [I>2σ(I)]	0.0228, 0.0546	0.0444, 0.0745
Final R$_1$, wR$_2$ (all data)	0.0270, 0.0572	0.0965, 0.0864
Flack parameter	-0.035(5)	
Largest diff. peak, hole (eÅ^3)	2.270, -1.459	1.426, -1.711

Results and Discussion

Synthesis and Structural Chemistry

The homoleptic bismuth carbamate $Bi(O_2CNPr^i_2)_3$ (**1**) was synthesised by the insertion of CO_2 into the

Bi-N bond of $Bi(NPr^i_2)_3$.[30] On bubbling dry CO_2 through a green solution of $Bi(NPr^i_2)_3$ in hexanes, there is

a colour change to pale yellow over a period of *ca*. 15 mins. Alternatively, the synthesis is also viable in

"one pot", by mixing $BiCl_3$, $LiNPr^i_2$ and bubbling CO_2 through the mixture without isolation of the $Bi(NPr^i_2)_3$

intermediate. The NMR of **1** is unexceptional, showing the expected doublet / septet pattern for the i-Pr

groups in the ^1H NMR and three resonances in the ^{13}C NMR (19.8, 44.4, 162.2 ppm), the most diagnostic

of which is the latter signifying the formation of the sp^2 NCO_2 centre.

Compound **1** is moderately air-sensitive and controlled exposure to moist air (by allowing a

concentrated solution of **1** to be exposed to the atmosphere over 2 days) leads to the crystallization of the

oxo-cluster $Bi_8(O)_6(O_2CNPr^i_2)_{12}$ (**2**).

$$Bi(NPr^i_2)_3 \xrightarrow{CO_2} Bi(O_2CNPr^i_2)_3 \xrightarrow{\text{moist air}} Bi_8(O)_6(O_2CNPr^i_2)_{12}$$
$$(\textbf{1}) \qquad\qquad\qquad\qquad (\textbf{2})$$

The ^1H NMR spectrum of **2** is complex, but shows that there are two distinct CH and three distinct CH_3

environments which persist in solution arising from restricted rotation about the $HC-CH_3$ bonds of the

peripheral i-Pr groups.
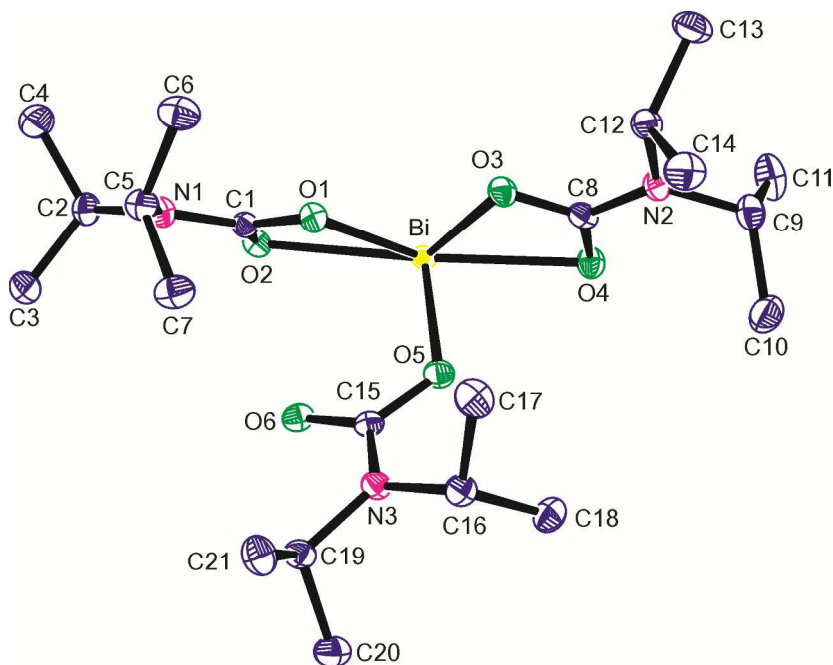
Figure 1.   The asymmetric unit of **1** showing the labelling scheme used; thermal ellipsoids are at the

40% probability level. The co-crystallised, disordered solvent molecule, modelled as

pentane, has been omitted for clarity. Selected metrical data: Bi-O(1) 2.217(2), Bi-O(2)

2.681(2), Bi-O(3) 2.227(2), Bi-O(4) 2.553(2), Bi-O(5) 2.232(2), Bi-O(6') 2.440(2), Bi-O2'''

2.813(2) Å.

The structure of **1** is shown in Figure 1, along with some selected bond length data. Each bismuth is

bonded to two chelating carbamate ligands while the remaining ligand bridges two metal centres. This

leads to an overall tetrameric species (Figure 2a), involving a non-planar sixteen-membererd $(BiOCO)_4$

ring; the overall shape of the tetramer is that of a box with the lid removed (Figure 2b). The geometry at

bismuth can be described as pentagonal bipyramidal, with the two Bi-O bonds associated with the

bridging carbamate [Bi-O(5) 2.232(2), Bi-O(6') 2.440(2) Å] occupying the axial sites and the bonds to the

chelating carbamates, including two of the weaker interactions [Bi-O(2) 2.681(2), Bi-O(4) 2.553(2) Å],

along with a void occupied by the lone pair, making up the equatorial girdle. The geometry is, however,

severely distorted, with additional long contacts which merit discussion. Firstly, an oxygen of one

chelating ligand forms long contacts with the symmetry-related metals either side [O(2)..Bi' 2.813(2);

O(2)…Bi''' 3.293(2) Å], of which only the shorter is shown in Fig. 2a. There is a further long, chelating

contact between bridging O(6) and bismuth [3.207(2) Å] but the orientation of the atoms makes this

interaction marginal at best; such an interaction, but at 3.27 Å, has been noted in $Bi(O_2CBu^t)_3$.[32] Indeed,

the structure **1** is comparable to that reported for. $Bi(O_2CBu^t)_3$ in that it too exists as cyclic tetrameric

units, with two terminal carboxylate ligands and one bridging carboxylate ligand per bismuth centre. For

comparison, in the carboxylate the oxygen which protrudes into the centre of the "box" is at 2.87 and 3.16
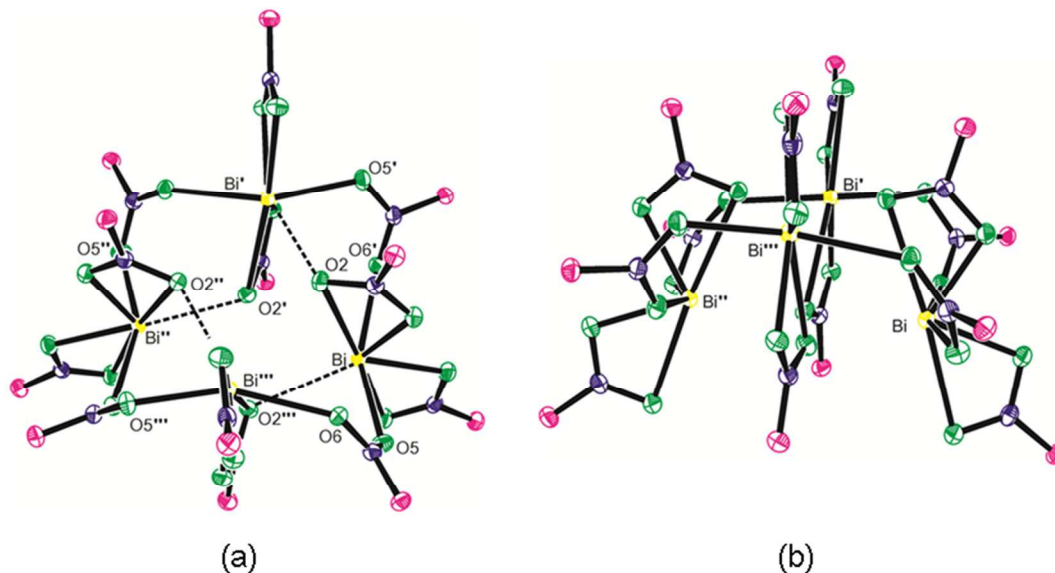
Å from the nearest metals.[32]

Figure 2.   Two views of the tetrameric aggregation of **1** (a) showing weak intermolecular contacts

between Bi and O2''' and (b) the non-planar nature of the ring. Symmetry operations: ' y, 1-

x, -z; '' 1-x, 1-y, z; ''' 1-y, x, 1-z.

   The composition of **1** in solution has been probed by DOSY NMR.[33] For a *ca*. 1 M solution in d_8-

toluene, the estimated molecular radius extracted from the diffusion coefficient using the Stokes-Einstein

equation is 6.5 Å, which is broadly consistent with a monomeric unit taken from the structure of the

tetramer (Bi-outer hydrogens *ca* 6.5 Å), though this is probably an overestimate of the size of a more

spherical tris-chelated monomer; for example, the radius of *tris*-(1-methoxy-2-methyl-2-propanolato-

O,O')bismuth(III) is in the range 4.4 – 5.1 Å.[34] Furthermore, the accuracy of radii derived from such DOSY

measurements is open to question.[35] However, both the ^{1}H and ^{13}C NMR spectra only show one

environment for the i-Pr groups at this concentration, which is also consistent with a *tris*-chelated

monomer, though a more complex, but fluxional entity would also show this behavior. For comparison, a

completely saturated solution shows very broad ^{1}H, ^{13}C NMR signals which may be indicative of some

association of monomers. Analysis of the DOSY data for this solution is compromised by these broad

signals and the tendency for the sample to start crystallizing from solution. The extrapolated molecular

radius from the solution at 353 K (to minimize crystallization) is *ca.* 10 Å, though this assumes the

viscosity of the solution is the same as pure d_8-toluene which may not be true given the high

concentration of solute. However, the collective data suggest that at high concentrations any equilibrium

between a monomer and the tetramer seen in the solid state is moving towards the latter. It should be

noted that the AACVD experiments were carried out on *ca*. 0.5 M solutions, and thus the "precursor

species" is almost certainly a monomeric unit.

The structure of **2** comprises a Bi_8O_6 core supported by twelve carbamate ligands (Figure 3). The

structure is complex, and comprises four distinct bismuth environments, five bonding modes for the

carbamate ligands and two types of oxo-bridges. Each of Bi(1), Bi(2) and Bi(4) is bonded to six oxygen

atoms in a distorted coordination sphere, with space evident which is presumably occupied by a lone

electron pair; though each metal also has an additional long Bi-O bond [Bi(1)-O(3): 3.058(4); Bi(2)-O(9')

2.951(4), Bi(4)-O(8) 2.798(4) Å]. Bi(3) has five short and one long Bi-O bond [Bi(3)-O(8') 2.813(4) Å]

again in a distorted coordination sphere with space occupied by a lone electron pair. Bi(1) is bonded to

one chelating carbamate, one μ_2-bridging carbamate, one μ_3-bridging carbamate, one μ_4-bridging

carbamate and two oxo-ligands, while Bi(2) is similarly ligated but with the chelating carbamate replaced

by a second μ_3-bridging ligand. Bi(3) is surrounded by four bridging carbamates (μ_2, two μ_3, μ_4) and two

oxo-ligands, while Bi(4), at the heart of the cluster, is bonded to three carbamates (two μ_3, μ_4) and four
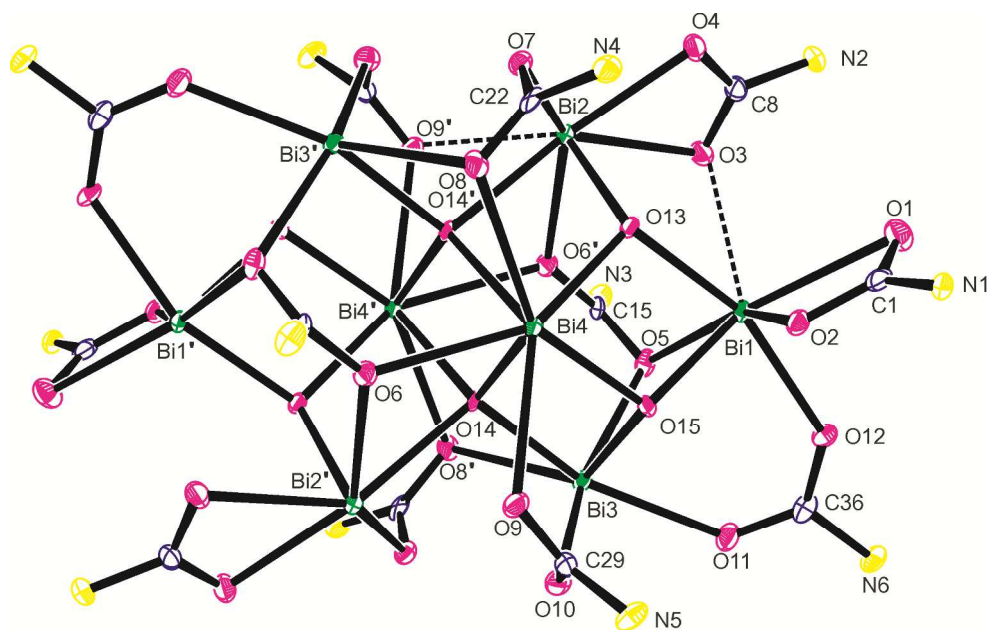
lone oxygen atoms.

Figure 3.   The asymmetric unit of **2** showing the labelling scheme used; thermal ellipsoids are at the

40% probability level. Selected metrical data: Bi(1)-O(1) 2.724(4), Bi(1)-O(2) 2.194(4),

Bi(1)-O(3) 3.058(4), Bi(1)-O(5) 2.703(4), Bi(1)-O(12) 2.320(4), Bi(1)-O(13) 2.251(4), Bi(1)-

O(15) 2.126(4), Bi(2)-O(3) 2.504(4), Bi(2)-O(4) 2.362(4), Bi(2)-O(6') 2.520(4), Bi(2)-O(7)

2.327(4), Bi(2)-O(9') 2.951(4), Bi(2)-O(13) 2.107(4), Bi(2)-O(14') 2.488(4), Bi(3)-O(5)

2.456(4), Bi(3)-O(8') 2.813(4), Bi(3)-O(10) 2.234(4), Bi(3)-O(11) 2.424(4), Bi(3)-O(14)

2.246(4), Bi(3)-O(15) 2.133(4), Bi(4)-O(6) 2.604(4), Bi(4)-O(8) 2.798(4), Bi(4)-O(9)

2.687(4), Bi(4)-O(13) 2.233(4), Bi(4)-O(14) 2.168(4), Bi(4)-O(14') 2.284(4), Bi(4)-O(15)

2.289(4) Å. Symmetry operation: 1-x, 1-y, -z.

The carbamate ligands divide between those which are purely chelating [e.g. κ^2-O(1)/O(2)], of which

there are two after symmetry considerations, those which bridge two metal centres [μ_2-O(11)/O(12), two

in total], four which bridge three bismuths [μ_3-O(7)/O(8) and O(9)/O(10)], two which bridge between four

metal centres [μ_4-O(5)/O(6) and its symmetry-related partner] and two which both chelate and bridge [$\mu_2,$

κ^2-O(3)/O(4)]; the oxo-ligands bridge metals in either a μ_3- [O(13,15)] or μ_4-manner [O(14)].

The overall geometry is too irregular to make anything other than general comments about the bond

lengths. Thus, the Bi-O bonds to the μ_2-brigding carbamates [2.242(4), 2.320(4) Å] are generally shorter

than those involving either the μ_4-carbamate ligands [2.456(4) – 2.703(4) Å], though the bonds involving

the μ_3-ligands are highly asymmetric [2.234(4), 2.327(4), 2.687(4) - 2.951(4) Å]. Similarly, Bi-O(μ_3) tend to

be shorter [2.107(4) – 2.289(4) Å] than those involving the μ_4-O [2.168(4) – 2.488(4) Å], though the

situation is less clearcut around Bi(4). The κ^2-ligand chelates very asymmetrically [2.149(4), 2.724(4) Å], a

situation which becomes more symmetrical in the μ_2, κ^2- ligand [2.362(4), 2.504(4) Å] when a long

bridging interaction is added [3.058(4) Å].

Only two other examples of Bi$_8$-oxo clusters are cited in a recent review,[5] namely $Bi_8(O)_4(OC_6F_5)_{16}$[36]

and $Bi_8(O)_4$(*p*-Bucalix[8]aren),[37] both of which show lower levels of hydrolysis than **2**; more recently, the

structure of $Bi_4(OH)_4(2,6\text{-pdc})_4(H_2O)_3 \cdot H_2O$ has been reported (2,6-pdc = 2,6 pyridine dicarboxylate), which

contains a linear $[Bi_8(2,6\text{-pdc})_8]^{8+}$ unit in which each metal is bridged by a $(2,6\text{-pdc})^{2-}$ ligand.[38] Small Bi-O

clusters have been rationalized in terms of the building blocks **A** – **C** (Scheme 1), which in turn are

generated from mononuclear $\mu_3\text{-OBi}_3$ and $\mu_4\text{-OBi}_4$ entities;[36] the aqueous chemistry of Bi salts is

dominated by the octahedron of metals in **A** ($[Bi_6O_8]^{2+}$, a motif common to hydroxyl and alkoxy

derivatives), and clusters with Bi_3, Bi_6 and Bi_9 are thus relatively common.[5] The structure of

$Bi_8(O)_4(OC_6F_5)_{16}$ is derived from **A** by the addition of two, exo-octahedral bismuth atoms, converting two

$\mu_3\text{-OBi}_3$ units into $\mu_4\text{-OBi}_4$.[36] $Bi_8(O)_4(p\text{-Bucalix}[8]\text{aren})$ is built from two **B** sub-units (a common feature of

many observed structures) rotated 90° to each other.[37] In contrast, the overall shape **2** can be described

as derived by the loss of one metal from **A** to generate the square-based pyramid of metals in **C** ($[Bi_5O_8]^-$),

two of which, inverted with respect to each other, fuse sharing a common edge (Fig. 4).
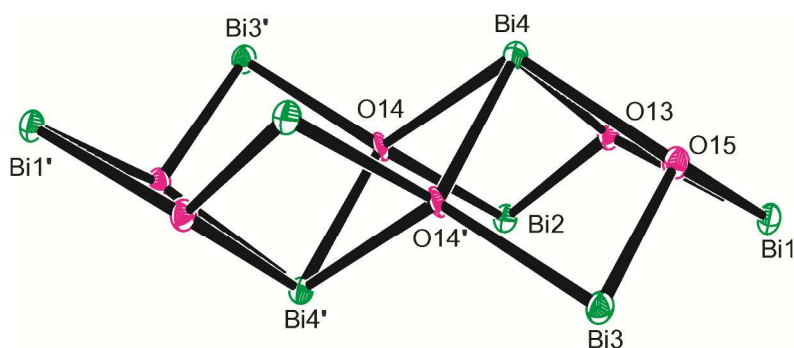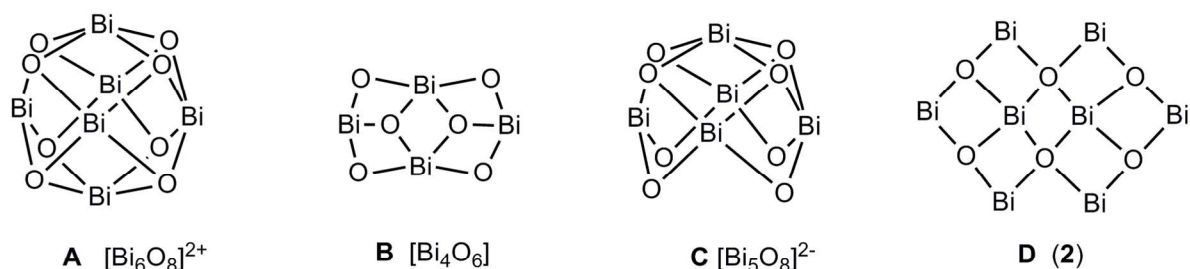

Figure 4.   The Bi_8O_6 core of **2**. Symmetry operation: 1-x, 1-y, -z.

In this respect, and in terms of formula, **2** is unique among the limited examples of other Bi_8 oxo-

clusters as the schematic of the core (**D**) highlights. This motif can, however, be discerned within

$[Bi_9(O)_8(OR)_6]^{5+}$[39] and the heterometallic cluster $Bi_{15}Na_3(O)_{18}(OSiMe_3)_{12}$.[40]

A $[Bi_6O_8]^{2+}$ **B** $[Bi_4O_6]$ **C** $[Bi_5O_8]^{2-}$ **D** (**2**)

Scheme 1

Materials Chemistry

Bismuth oxide is a remarkable material, occurring in five polymorphic forms (α, β, γ, δ and ω) of which

the α- and δ-forms are considered stable while the others are metastable.[41, 42] Each modification has its

own properties, for example the bandgap for Bi_2O_3 ranges from 2.0 eV (amorphous) to 2.85 eV (α), while

BiO has a bandgap of 3.31 eV;[41] other authors report band gaps of 2.84 – 2.90 (α), 2.55 – 2.75 (β), 2.68 –

2.80 (γ) and 2.93 – 3.10 (δ)[43] though a wider spread of values than this can be found.[44]
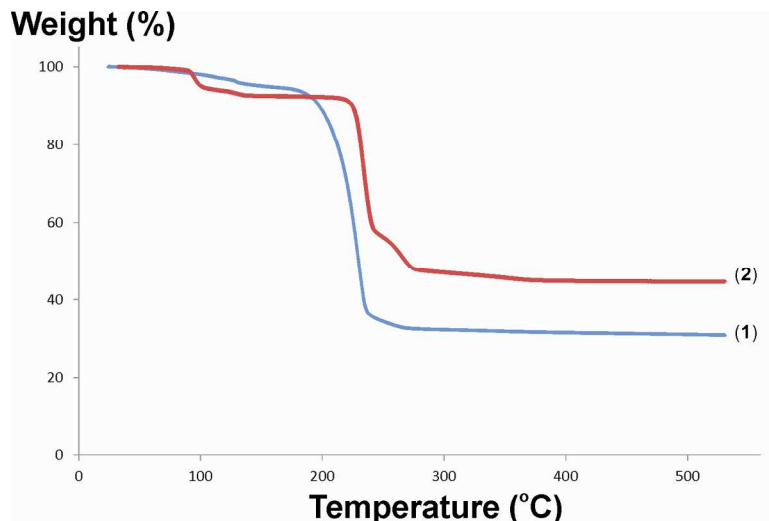
Figure 5.   TGA of **1** and **2**.

The TGA of **1** and **2** is shown in Figure 5. For **1**, the residual mass at 300 $^{\circ}$C (32.2%) is consistent with

Bi_2O_3 formation (theoretical residual mass 34.4%), indeed the consistency is negatively compromised

slightly by a small amount of residual solvent loss (ca. 2%) at the outset of the pyrolysis. Similarly, data

for **2** show initial loss of lattice THF (theoretical loss for 6 THF per Bi_8 cluster 11.0%, observed 7.4% at 150 ^{o}C), the discrepancy probably arising from some loss of lattice THF on drying the material after synthesis; the %weight change between 150 – 400 ^{o}C (47.7%) is consistent with the transformation $Bi_8(O)_6(O_2CNPr^i_2)_{12} \rightarrow 4Bi_2O_3$ (theoretical % loss 46.7%). Films of bismuth oxide have been deposited using **1 as** precursor, by aerosol-assisted chemical vapour deposition (AACVD) onto glass substrates at temperatures between 300 and 450 ^{o}C (R1 – R4) and the outcomes analysed by PXRD (Figure 6), AFM (Figure 7) and SEM (Figure 8). At 300 ^{o}C over a 10 mins deposition time (R1), a hard, light brown/yellow, transparent film was produced which was strongly adhered to the glass substrate; PXRD can be indexed to the cubic δ-modification of Bi_2O_3 (Figure 6a). The film is smooth and featureless making it hard to image, but can be clearly seen in the SEM (edge view) of the film grown at the same temperature over a longer period (Figure 8a; *see below*) and is *ca.* 300 nm in thickness. This is in marked contrast to the elaborate hierarchical structures obtained by base hydrolysis of $Bi(NO_3)_3$ / NH_4VO_3 mixtures.[45] AFM analysis of this growing film shows that, after 5 mins the film comprises particles of dimension *ca.* 20 nm (Figure 7a,b), which become less well-defined after 10 mins growth time (Figure 7c,d); the estimated roughness of the films is *ca.* 6 nm. A similar morphology has been observed for β-Bi_2O_3 grown by dip coating a solution of $Bi(NO_3)_3$ / 2-methoxyethanol and the organic template $(CH_2CH_2)_{0.67}(CH_2CHCH_2CH_3)_{0.33}]_{89}(OCH_2CH_2)_{79}OH$ and calcined at 400 ^{o}C.[46]
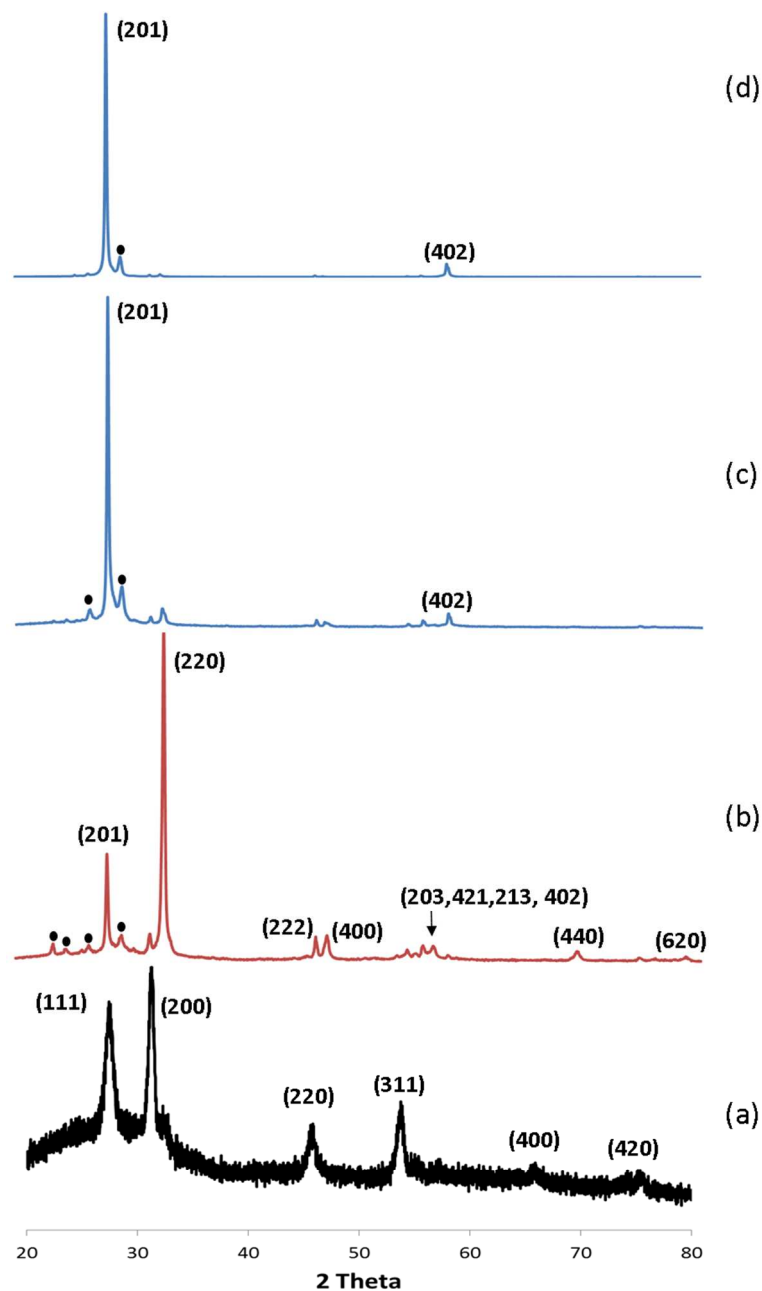
Figure 6.   PXRD plots of the films grown from **1;** bottom upwards (a) deposition at 300 ^{o}C for 10 mins

(R1), (b) deposition at 300 ^{o}C for 40 mins (R2), (c) deposition at 375 ^{o}C for 40 mins (R3)

and (d) deposition at 450 ^{o}C for 40 mins (R4). In (a), indexing is to cubic δ-Bi_2O_3 (PDF 77-

2008), (b-d) indexed to tetragonal Bi_2O_3 (PDF 78-1793), with $\bullet$ attributed to $Bi_2O_{2.73}$ (PDF

76-2477) and the residue of δ-Bi_2O_3 visible but unlabelled in (b).
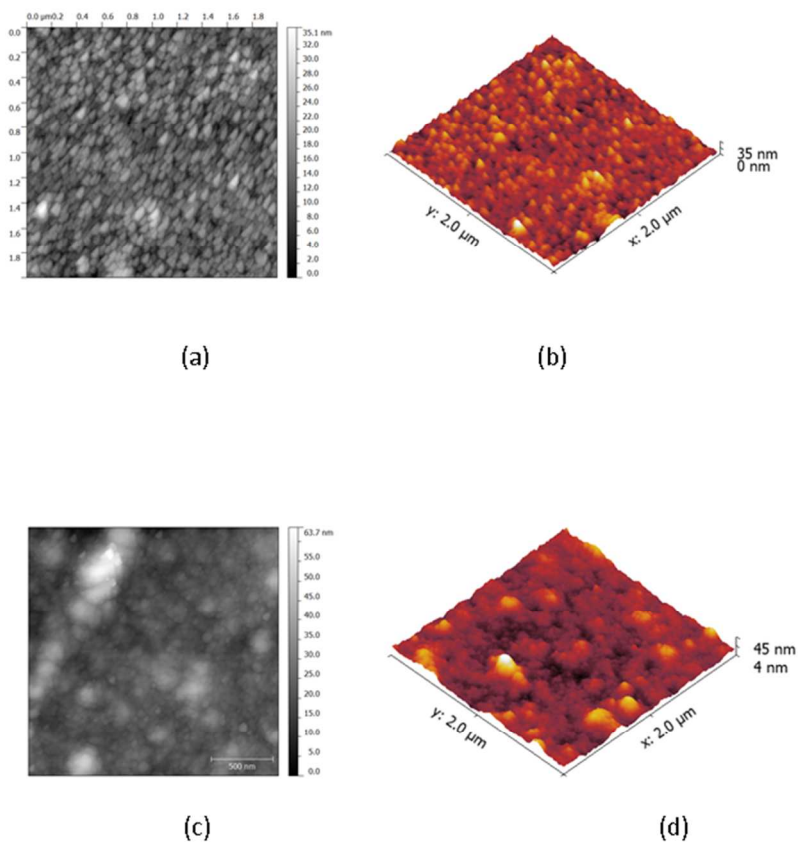
(a) (b)

(c) (d)

Figure 7.   AFM analysis of the film grown from **1** at 300 °C after (a,b) 5 mins and (c,d) 10 mins

deposition time. In each case the images cover a 2 x 2 μm region of the film.
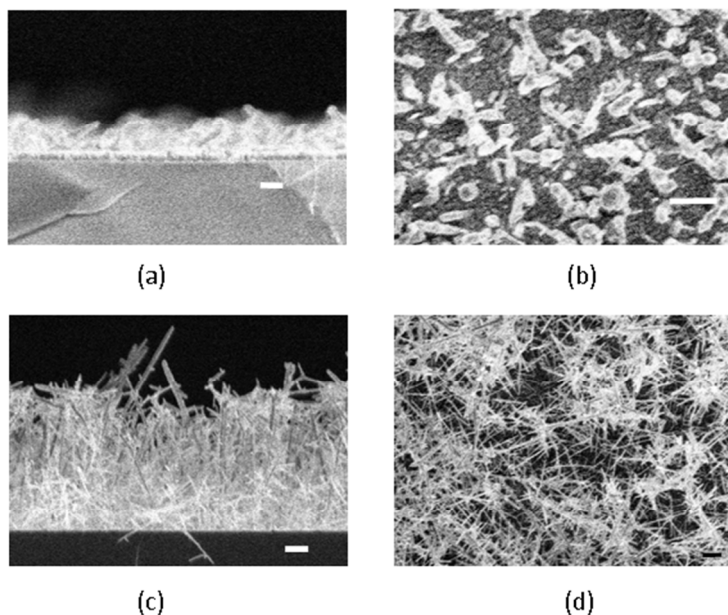
Figure 8.   SEM of the films grown from **1**, (a,b) at 300 $^{\circ}$C for 40 mins (R2) and (c,d) at 450 $^{\circ}$C for 40

mins (R4); bar = 1 μm in all images

When the run time is extended to 40 mins (R2), the film has a more powdery, bright yellow

appearance and is poorly adhered to the glass. The PXRD is dominated by reflections which can be

indexed to tetragonal β-Bi$_2$O$_3$ with some preferential orientation in the (220) direction, this latter reflection

appearing significantly more intense than that of (201), the dominant line in the random pattern; the

underlying δ-Bi$_2$O$_3$ is still visible in the PXRD pattern, along with traces of sub-stoichiometric Bi$_2$O$_{2.73}$

(Figure 6b). SEM of this film (Figure 8a,b) show both the hard underlying δ-Bi$_2$O$_3$ (*ca*. 300 nm thick) and

the growth of a more needle-like material above it (*ca*. 1 μm in height). It would seem that at 300 $^{\circ}$C the

formation of δ-Bi$_2$O$_3$ provides a template on which β-Bi$_2$O$_3$ grows. At 375 $^{\circ}$C (R3) and 450 $^{\circ}$C (R4), only β-

Bi$_2$O$_3$ is visible in the PXRD (save for traces of Bi$_2$O$_{2.73}$), with an increasing degree of preferred (201)

orientation as the temperature is raised (Figures 6c, d). The base film of δ-Bi$_2$O$_3$ is still discernible in the

image of the film grown at 450 $^{\circ}$C (though it is now in such a relatively small amount as to not register in

the PXRD of Figure 6d), which is now dominated by β-Bi$_2$O$_3$ fibres growing to *ca*. 5 μm in height (Figure

8c,d). Similar β-Bi$_2$O$_3$ nanowires have been deposited on aluminium at 300 $^{\circ}$C by O$_2$ oxidation of bismuth

powder heated to 800 ^{o}C over an 8 h period under an N$_2$ flow; however, under the same conditions at a

substrate temperature of 500 ^{o}C the α-modification is formed.[47]

The most stable modifications of Bi$_2$O$_3$ are monoclinic α (up to 729 ^{o}C) and cubic δ (stable up to 824

^{o}C), with metastable β- and γ-forms appearing on cooling at T *ca.* 600 – 650 ^{o}C.[48] However, CVD

produces all four modifications across a range of temperatures, in which the modification adopted seems

to depend on the precursor rather than temperature control (Table 2). Deposition using **1** affords the δ-

modification, an excellent oxide ion conductor and the phase with the highest conductivity,[49] at the lowest

temperature yet reported, with no evidence for the formation of either the α- or γ-modifications. The β-

modification, which is dominant at both higher temperatures and at lower temperatures over an extended

run time, also has good oxide ion conductivity, surpassing that of yttria-stabilised zirconia (YST). The

formation of small amounts of sub-stoichiometric Bi$_2$O$_{2.73}$ is, perhaps, not surprising given **1** is acting as a

true SSP.

Table 2. Bi_2O_3 phases and deposition temperatures for CVD-grown bismuth oxide [a]

	BI_3 / O_2	$BiPh_3 / O_2$	$BiMe_3 / O_2$	$Bi(thd)_3 / O_2$	$Bi(OCMe_2Et)_3$	$Bi(OBu^t)_3$	**1** (this work)
200				amorphous [26 b]			
250				α [26 b]			
300				amorphous [25]			$\beta + \delta$ [c, d]
375							β [d]
400		β [20]					
420, 425		$\alpha + \beta$ [22 e]				β [28]	
450		γ + trace β [20 f]	α [24]	β [23]		α,β,γ [28 e]	β [d]
400-750							
500		α [20]					
550				α [25]			
600					α, γ [29]		
600-800	$Bi_2O_{2.33}$ [12]						
700				γ [26 b]			
800	δ [14-16, 18]						

[a] Deposition or annealing temperature depending on when the sample was analysed by PXRD. [b] ALD. [c] time dependent. [d] traces $Bi_2O_{2.73}$ are also seen. [e] product depends on gas flow rate, co-reactant H_2O. [f] o,p-$(CH_3C_6H_4)_3Bi$ deposit β modification at 450 °C.[23]

The photocatalytic activity of bismuth oxide is well documented, with α-,[47, 50-52] β-[46, 47, 52-55] and

δ-polymorphs[45] being active, though the β-modification is considered the most active. In this work,

single-phase δ-Bi_2O_3 has been assessed by the degradation of methylene blue dye; a parallel

experiment under similar conditions was carried out using a commercially marketed sample of

TiO_2 on glass (NSG / Pilkington Active™) for comparison (Figure 9).
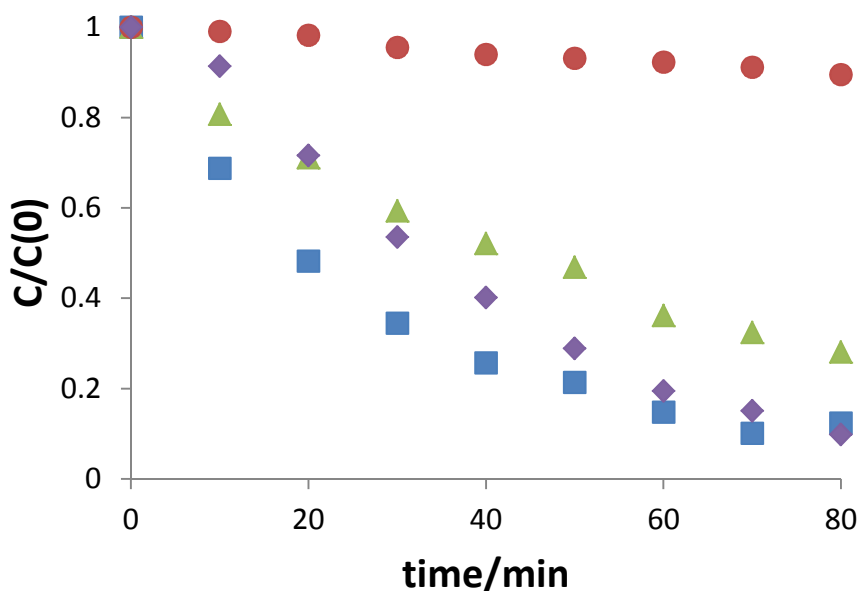

Figure 9.   Photodegradation of only methylene blue dye (•), methylene blue dye using (♦)

TiO_2 (NSG / Pilkington Activ™), (▪) δ-Bi_2O_3 thin film and (▲) δ-Bi_2O_3 thin film

overcoated with β-Bi_2O_3 nanowires, all under a 200 W HMI HR lamp; C =

concentration, C(0) = concentration at time 0 sec.

The 300 nm thin film of δ-Bi_2O_3 deposited from **1** over a 10 min period at 300 ^{o}C (R1, *above*)

shows a very similar level of photocatalytic activity to commercial TiO_2-coated glass, while, in

contrast, that of the film deposited over a 40 min period at 450°C – β-Bi_2O_3 nanowires grown over

the same δ-Bi_2O_3 base (R4, *above*; Figure 8c,d) – were less active. It was noted that (i) despite

their visual fragility the majority of nanowires appear to remain adhered to the underlying δ-Bi_2O_3

film during the photodegradation experiment, but (ii) the wettability of the nanowires was significantly less than that of the δ-Bi$_2$O$_3$ film, as reflected in contact angles of 73° and 137° for the δ- and β-Bi$_2$O$_3$ films, respectively (Figure 10). Thus it seems likely that the lower photoactivity of the β-Bi$_2$O$_3$ nanowires seems to be related to the poor interface between the catalyst and the aqueous solution in this system, which in turn can be attributed to the morphology of the as-deposited material.
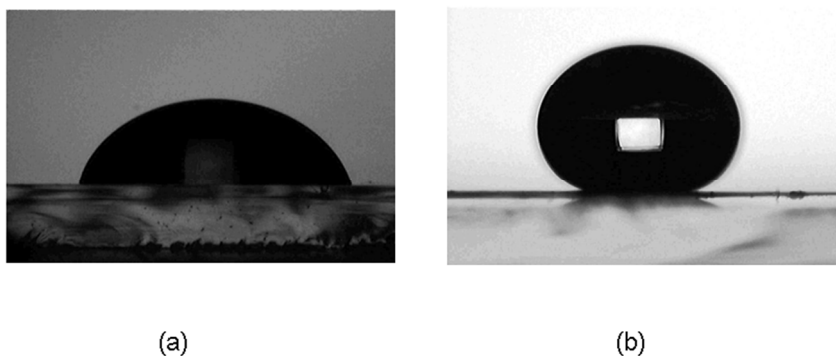

(a)   (b)

Figure 10.   Contact angles of a water droplet on (a) δ-Bi$_2$O$_3$ (b) β-Bi$_2$O$_3$.

Conclusions

The bismuth carbamate Bi(O$_2$CNPr$^i_2$)$_3$ (**1**) has proved a versatile precursor for the deposition of differing modifications of Bi$_2$O$_3$ films on glass, depending on the duration and temperature of the deposition process, providing a degree of control between δ- and β-Bi$_2$O$_3$. The δ-Bi$_2$O$_3$ films show good catalytic activity (comparable to commercial TiO$_2$ NSG / Pilkington Activ™), and better than that of the deposited β-Bi$_2$O$_3$ nanowires, which have a much higher water droplet contact angle. Controlled exposure of **1** to atmospheric moisture yields the novel octa-bismuth cluster Bi$_8$(O)$_6$(O$_2$CNPr$^i_2$)$_{12}$ (**2**).

Supporting Information

Crystallographic data for the structural analysis (in CIF format) have been deposited with the Cambridge Crystallographic Data Centre, CCDC nos. 940280, 940281 for **1**, **2**, respectively. Copies of this information may be obtained from the Director, CCDC, 12 Union Road, Cambridge, CB21EZ, UK (Fax: +44-1233-336033; e-mail: deposit@ccdc.cam.ac.uk or www.ccdc.cam.ac.uk).

References

1.   D. Belli Dell'Amico, F. Calderazzo, L. Labella, F. Marchetti and G. Pampaloni, *Chem. Rev.*, 2003, **103**, 3857

2.   F. Ando, T. Hayashi, K. Ohashi and J. Koketsu, *J. Inorg. Nucl. Chem.*, 1975, **37**, 2011.

3.   A. J. Petrella, H. Deng, N. K. Roberrs and R. N. Lamb, *Chem. Mater.*, 2002, **14**, 4339.

4.   R. Pothiraja, A. P. Milanov, D. Barreca, A. Gasparotto, H.-W. Becker, M. Winter, R. A. Fischer and A. Devi, *Chem. Commun.*, 2009.

5.   M. Mehring, *Coord. Chem. Revs.*, 2007, **251**, 974.

6.   J. Wu, F. Huang, P. Chen, D. Wan and F. Xu, *J. Mater. Chem.*, 2011, **21**, 3872.

7.   P. C. Andrews, P. C. Junk, I. Nuzhnaya and D. T. Thielemann, *Inorg. Chem.*, 2012, **51**, 751.

8.   R. Palai, J. F. Scott and R. S. Katiyar, *Phys. Rev. B*, 2010, **81**, 064110.

9.   S. W. Kang and S. W. Rhee, *J. Mater. Sci.: Mater. Electron.*, 2004, **15**, 231.

10.   S. W. Kang, K. J. Yang, K. J. Yong and S. W. Rhee, *J. Electrochem. Soc. India*, 2002, **149**, C44.

11.   H. Raffy, in *High-temperature superconductors*, ed. X. G. Qui, Woodhead, Cambridge, UK, 2012.

12.   M. Schuisky and A. Harsta, *Chem. Vapor Depos.*, 1996, **2**, 235.

13.   T. Takeyama, N. Takahashi, T. Nakamura and S. Ito, *Optical Materials*, 2004, **26**, 413.

14.   T. Takeyama, N. Takahashi, T. Nakamura and S. Ito, *J. Phys. Chem. Solids*, 2004, **65**, 1349.

15.   T. Takeyama, N. Takahashi, T. Nakamura and S. Itoh, *J. Cryst. Growth*, 2005, **277**, 485.

16.   T. Takeyama, N. Takahashi, T. Nakamura and S. Itoh, *J. Cryst. Growth*, 2005, **275**, 460.

17.   T. Takeyama, N. Takahashi, T. Nakamura and S. Itoh, *Solid State Commun.*, 2005, **133**, 771.

18.   T. Takeyama, N. Takahashi, T. Nakamura and S. Itoh, *Surf. Coat. Technol.*, 2006, **200**, 4797.

19.   T. N. Soitah, C. Yang, Y. Yu, Y. Niu and L. Sun, *Current Applied Physics*, 2010, **10**, 1372.

20.   C. Bedoya, G. G. Condorelli, G. Anastasi, A. Baeri, F. Scerra, I. L. Fragala, J. G. Lisoni and D. Wouters, *Chem. Mater.*, 2004, **16**, 3176.

21.   N. Reuge, J. Dexpert-Ghys and B. Caussat, *Chem. Vapor Depos.*, 2010, **16**, 123.

22.   G. Bandoli, D. Barreca, E. Brescacin, G. A. Rizzi and E. Tondello, *Chem. Vapor Depos.*, 1996, **2**, 238.

23.   C. Bedoya, G. G. Condorelli, S. T. Finocchiaro, A. Di Mauro, I. L. Fragala, L. Cattaneo and S. Carella, *Chem. Vapor Depos.*, 2005, **11**, 261.

24.   H. W. Kim, J. H. Myung, S. H. Shim and C. Lee, *Appl. Phys. A - Mat. Sci. & Proc*, 2006, **84**, 187.

25.   S. W. Kang and S. W. Rhee, *Thin Solid Films*, 2004, **468**, 79.

26.   Y. D. Shen, Y. W. Li, W. M. Li, J. Z. Zhang, Z. G. Hu and J. H. Chu, *J. Phys. Chem. C*, 2012, **116**, 3449.

27.   P. A. Williams, A. C. Jones, M. J. Crosbie, P. J. Wright, J. F. Bickley, A. Steiner, H. O. Davies, T. J. Leedham and G. W. Critchlow, *Chem. Vapor Depos.*, 2001, **7**, 205.

28.   S. J. A. Moniz, C. S. Blackman, C. J. Carmalt and G. Hyett, *J. Mater. Chem.*, 2010, **20**, 7881.

29.   M. A. Matchett, M. Y. Chiang and W. E. Buhro, *Inorg. Chem.*, 1990, **29**, 358.

30.   M. Vehkamaki, T. Hatanpaa, M. Ritala and M. Leskela, *J. Mater. Chem.*, 2004, **14**, 3191.

31.   L. J. Farrugia, *J. Appl. Crystallogr.*, 1999, **32**, 837.

32. S. I. Troyanov and A. P. Pisarevskii, *Chem. Commun.*, 1993, 335.

33. A. L. Ward, H. L. Buckley, W. W. Lukens and J. Arnold, *J. Am. Chem. Soc.*, 2013, **135**, 13965.

34. P. A. Williams, A. C. Jones, M. J. Crosbie, P. J. Wright, J. F. Bickley, A. Steiner, H. O. Davies, T. J. Leedham and G. W. Critchlow, *Chem.Vap.Deposition*, 2001, **7**, 205.

35. R. Evans, Z. Deng, A. K. Rogerson, A. S. McLachlan, J. J. Richards, M. Nilsson and G. A. Morris, *Angew. Chem. Int. Ed.,*, 2013, **52**, 3199.

36. K. H. Whitmire, S. Hoppe, O. Sydora, J. L. Jolas and C. M. Jones, *Inorg. Chem.*, 2000, **39**, 85.

37. L. Liu, L. N. Zakharov, A. L. Rheingold and T. A. Hanna, *Chem. Commun.*, 2004, 1472.

38. X.-P. Zhang, H.-R. Tian, G.-F. Yan, Y. Su, Y.-L. Feng and J.-W. Cheng, *Dalton Trans.*, 2012, **42**, 1088.

39. J. H. Thurston, D. C. Swenson and L. Messerle, *Chem. Commun.*, 2005, 4228.

40. M. Mehring, S. Paalasmaa and M. Schürmann, *Eur. J. Inorg. Chem.*, 2005, 4891.

41. L. Leontie, M. Caraman, M. Alexe and C. Harnagea, *Surf. Sci.*, 2002, **507-510**, 480.

42. H. A. Harwig, *Z. Anorg. Allg. Chem.*, 1978, **444**, 151.

43. E. Li, C. Lang, Z. Qiang, L. Wenhua and Y. Shuangfeng, *Prog. in Chem.*, 2010, **22**, 2282.

44. B. Sirota, J. Reyes-Cuellar, P. Kohli, L. Wang , M. E. McCarroll and S. M. Aouadi, *Thin Solid Films* 2012, **520**, 6118.

45. L. Zhou, W. Wang, H. Xu, S. C. Sun and M. Shang, *Chem. Eur. J.,*, 2009, **15**, 1776.

46. K. Brezesinski, R. Ostermann, P. Hartmann, J. Perlich and T. Brezesinski, *Chem. Mater.*, 2010, **22**, 3079.

47. Y. Qiu, M. Yang, H. Fan, Y. Zuo, Y. Shao, Y. Xu, X. Yanga and S. Yang, *CrystEngComm*, 2011, **13**, 1843.

48. P. Shuk, H.-D. Wiemhöfer, U. Guth, W. Göpel and M. Greenblatt, *Solid State Ionics*, 1996, **89**, 179.

49. H. A. Harwig and A. G. Gerards, *J. Solid State Chem.*, 1978, **26**, 265.

50. S. Iyyapushpam, S. T. Nishanthi and D. PthinettamPadiyan, *Mater. Lett.*, 2012, **86**, 25.

51. M. Muruganandham, R. Amutha, G.-J. Lee, S.-H. Hsieh, J. J. Wu and M. Sillanpaa, *J. Phys. Chem. C*, 2012, **116**, 12906.

52. W. He, W. Qin, X. Wu, X. Ding, L. Chen and Z. Jiang, *Thin Solid Films*, 2007, **515**, 5362.

53. M. Schlesinger, S. Schulze, M. Hietschold and M. Mehring, *Dalton Trans.*, 2013, **42**, 1047.

54. J. B. Zhong, X. Y. He, J. Z. Li, J. Zeng, Y. Lu and W. Hu, *J. Adv. Oxid. Technol.,* 2012, **15**, 334.

55. M. Schlesinger, M. Weber, S. Schulze, M. Hietschold and M. Mehring, *ChemistryOpen*, 2013, **2**, 146.

1
2
3
4
5
6
7
8
9
10
11
12
13
14
15
16
17
18
19
20
21
22
23
24
25
26
27
28
29
30
31
32
33
34
35
36
37
38
39
40
41
42
43
44
45
46
47
48
49
50
51
52
53
54
55
56
57
58
59
60

TOC Synopsis and Graphical Abstract

δ- and β-Bi$_2$O$_3$ thin films can be deposited by AACVD from a Bi(O$_2$CNPr$^i_2$)$_3$ precursor, with temperature and temporal control over the deposition process. Thin δ-Bi$_2$O$_3$ films show good catalytic activity towards the photodegradation of methylene blue, while β-Bi$_2$O$_3$ nanowires are less active due to an increased hydrophobicity. Controlled hydrolysis of Bi(O$_2$CNPr$^i_2$)$_3$ affords the novel oxo-cluster Bi$_8$(O)$_6$(O$_2$CNPr$^i_2$)$_{12}$.

Bi(O$_2$CNPr^i)$_3$

H$_2$O   AACVD

Bi$_8$(O)$_6$(O$_2$CNPr$^i_2$)$_{12}$ **δ- and β-Bi$_2$O$_3$**